Droplets sliding on fibres

T. Gilet[1], D. Terwagne[2], and N. Vandewalle[2]

[1] Department of Mathematics, Massachusetts Institute of Technology, Cambridge, MA 02139, USA

[2] GRASP, University of Liege, 4000 Liege, Belgium

Abstract. We present the results of a combined experimental and theoretical investigation of oil droplets sliding on fibres. First, both the axisymmetric shape and the motion of a droplet on a vertical fibre are described. The motion is shown to result from a balance between the droplet weight and the viscous stresses. On a long-term range, the droplet loses some mass through coating the fibre, which decreases its velocity. In a second time, we rationalize the behaviour of a droplet that encounters a junction between vertical and horizontal fibres. Depending on its size, the droplet may cross the junction or remain blocked. The transition is well-described by an ordinary differential equation equivalent to a damped harmonic oscillator truncated to the neighbourhood of the horizontal fibre. This simple system is the basic element for more complex fiber networks that would be useful in microfluidic applications involving droplets.

PACS. PACS-key discribing text of that key – PACS-key discribing text of that key

1 Introduction

In the early morning, the spider webs in our gardens are often covered with a myriad of dew pearls. At dawn, the fresh and humid air condenses into a thin water film on the threads. Quickly, this film turns into a string of droplets, the smallest of which stay on the web and wait for the first sunbeams to evaporate again. The biggest slide and roll along the web (Fig. 1), collide and fuse together, leave pearls in their wake, and sometimes fall from the web. Can these 'arachnidean' constructions inspire new directions for microfluidics?
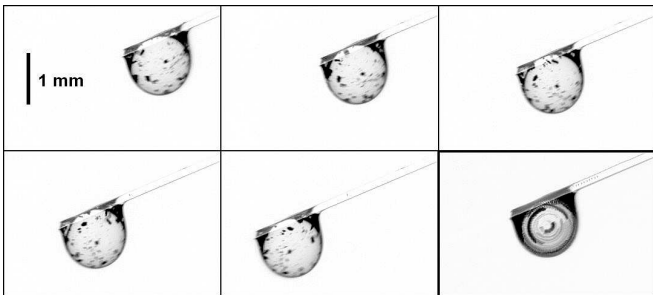

Fig. 1. An oil droplet ($\nu = 100$ cS) slides and rolls along a fibre of diameter 140 μm. Snapshots are taken every 50 ms. The background, including the originally dry fibre, is subtracted in order to reveal the micrometric coating film left in the wake of the droplet. The last picture corresponds to the sum of the formers; the particles within the droplet follow some circular paths, indicating that the droplet rolls on the fibre.

Droplets on fibres are omnipresent in nature, they are already involved in many applications, e.g. the microscale alignment of fibres [21] or the clogging of fibre filters [4, 26]. Nevertheless, since the pioneering work of Joseph Plateau [18], physicists have rather investigated the flows of liquid films on threads [10, 5, 8] and a relatively small number of studies were dedicated to the interactions between individual droplets and fibres. Plateau [18] has already observed that, due to surface tension only, a liquid covering a fibre spontaneously turns into a string of pearls called unduloid. A similar instability is observed for falling cylindrical jets, as rationalised a few years later by Lord Rayleigh [20]. The instability of a thin film on a fiber is developed extensively in Yarin *et al.* [27] and references therein. Nevertheless, droplets may take other shapes than the one proposed by Plateau. For example, the axisymmetry of the shape is broken down by gravity for large droplets on a horizontal fibre. If the liquid does not perfectly wet the fibre (e.g. pure water on nylon), the droplet cowers on one side of the fibre without wrapping it [3, 17]. Such droplets often hang at rest on a vertical fibre [11]; their weight is balanced by a bottom-up difference in contact angle. Tiny droplets may be set into motion on horizontal fibres in several ways, e.g. with temperature gradients [25], thanks to a gas flow [6], or when the fibre is conical [16]. Sliding droplets have also been studied in other geometries, e.g. on an inclined plane [13, 22] or as slugs in a tube [2].

In this manuscript, we observe experimentally the gravity-induced motion of droplets on fibre networks, focusing on droplets that perfectly wet the fibres and slide on them. In section §3, we start by rationalising the behaviour of a droplet sliding on a vertical fibre thanks to gravity.
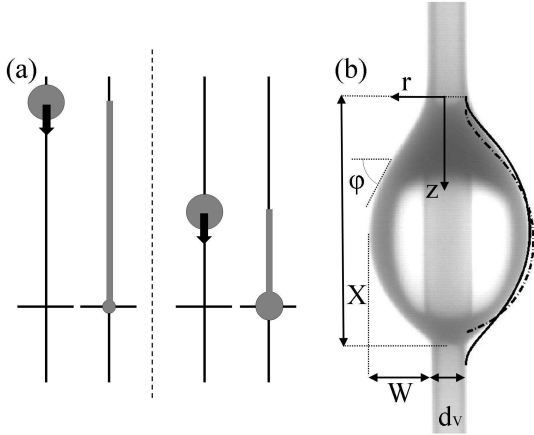
Fig. 2. (a) The droplet size is tuned by changing the height of release and so the coating length. (b) Axisymmetric shape of an oil droplet on a vertical nylon fibre. The dash-dotted and solid lines correspond to the numerical solutions of Eq.(1) with and without the gravity term respectively.

We proceed in §4 by observing the interaction between a droplet and an intersection between two fibres.

2 Experimental method

Fibers made of nylon (fishing thread) are tight on a metallic frame. The tension in the fibres is supposed to be of negligible influence on the droplet motion. Droplets are made of silicon oil (Dow Corning 200) though the results may be generalised to any liquid that completely wets the fibre. Experiments involve fibres of 5 different diameters (80, 100, 140, 200 and 250 μm) and droplets with six different kinematic viscosities ν (1.5, 5, 10, 20, 50 and 100 cS); the corresponding density ρ is respectively (0.85, 0.91, 0.93, 0.95, 0.96 and 0.96 g/cm^3). Droplets are directly released on the fibres with a syringe. The droplet size is varied by changing the needle diameter. Moreover, moving the release point on the fibre allows to tune the volume of the droplet when it enters a specified region of interest. Indeed, as explained below, the droplet loses some mass by coating the fibre; so the greater the distance between the release point and the region of interest, the smaller the resulting droplet (Fig. 2a). About 500 droplets have been filmed from the side with a high-speed camera (recording frequency up to 1000 fps). Measurements are made by image processing (Fig. 2b).

3 A droplet sliding on a vertical fibre

3.1 Geometry

On a vertical fibre of diameter d_v, wetting droplets take an axisymmetric shape of volume Ω, close to the unduloid of Plateau (Fig. 2b), dimensions (width W and extension X)

of which are represented as a function of Ω in Fig. 3(a-b). This shape is computed theoretically as $[r(s), z(s), \varphi(s)]$, where s is the curvilinear coordinate along a meridian of the interface (Fig. 2b). If we suppose a balance between gravity g and surface tension σ, the Laplace equation yields

$$\begin{cases} \mathrm{d}_s r = \cos \varphi, \\ \mathrm{d}_s z = \sin \varphi, \\ \mathrm{d}_s \varphi = \dfrac{P}{\sigma} - \dfrac{\sin \varphi}{r} + \dfrac{z}{\lambda_\sigma^2}, \end{cases} \tag{1}$$

where P is the overpressure within the droplet at location $z = 0$, and $\lambda_\sigma = \sqrt{\sigma/\rho g}$ is the capillary length. Nevertheless, if this balance of gravity and surface tension was effective, the droplet would stay at rest on the fibre. The observed sliding of the droplet suggests that viscous stresses have to be taken into account. Therefore, we may suppose that these stresses balance gravity, and that surface tension forces balance themselves. To assess this hypothesis, Eq. (1) is solved numerically as an initial value problem, the boundary condition in $s = 0$ being $r(0) = d_v/2$, $z(0) = 0$ and $\varphi(0) = \pi/2$. The integration is stopped as soon as $r = d_v/2$ again. The scenarios including and neglecting the gravity term z/λ_σ^2 are considered successively. The comparison with measurements (Fig. 2b and 3b) clearly confirms this second scenario. The solution taking gravity into account cannot explain vertical extensions X as large as those observed experimentally. Gravity can thus be neglected in the Laplace equation and the unduloid is a good approximation for the droplet shape.

Although the unduloid cannot be described with a simple explicit equation, it is possible to find some analytical expressions in the asymptotic regimes $\Omega \gg d_v^3$ and $\Omega \ll d_v^3$. Large droplets ($\Omega/d_v^3 > 10^4$) tend to keep their spherical shape when they are hanged on a fibre. The sphere of radius R, described by $(r_0, z_0, s_0) = R(\sin \varphi, 1 - \cos \varphi, \varphi)$ satisfies Eq. (1) for $\Delta p = 2\sigma/R \ll 1$ but not matching conditions on the fibre. On the other hand, the matching zone involves a very small amount of liquid so the volume of the droplet is approximately equal to the volume of the sphere. Therefore, we infer

$$\frac{W}{d_v} \simeq \left(\frac{3\Omega}{4\pi d_v^3} \right)^{1/3} \quad \text{and} \quad X = 2W. \tag{2}$$

These scalings are similar to those discussed in Lorenceau *et al.* [16]. When the droplet size is smaller than d_v, the droplet spreads on the fibre in such a way that the curvature of its interface is only slightly lower than the fibre curvature $2/d_v$. Therefore, we can infer the asymptotic solution by perturbing the solution $(r_0, z_0, \varphi_0) = (d_v/2, s, \pi/2)$ when $\Omega = 0$ (corresponding to the fibre itself). Supposing that $\Delta p = 2\sigma(1 - \varepsilon)/d_v$ and that the perturbations are denoted by tilted variables, we obtain

$$\begin{cases} \mathrm{d}_s \tilde{r} \simeq -\tilde{\varphi}, \\ \mathrm{d}_s \tilde{z} \simeq 0, \\ \mathrm{d}_s \tilde{\varphi} \simeq \dfrac{4\tilde{r}}{d_v^2} - \dfrac{2\varepsilon}{d_v}, \end{cases} \tag{3}$$
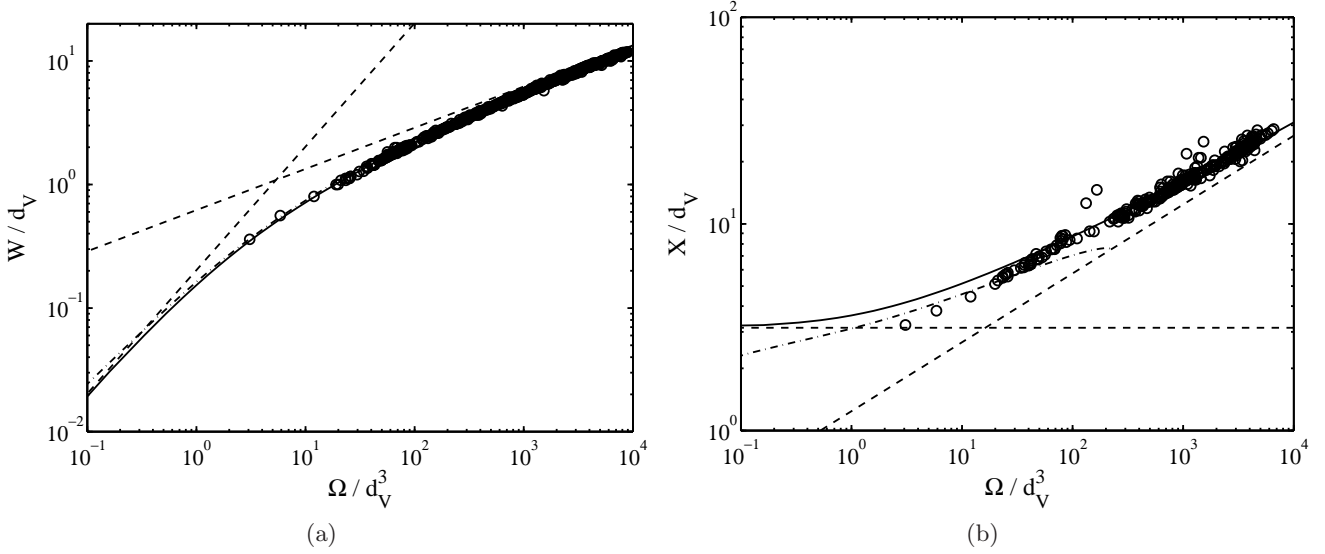
Fig. 3. (a) Width W and (b) extension X of a droplet of volume Ω on a fibre of diameter d_v. The dashed line represents the asymptotic scalings (2) and (5). The solid line (resp. dash-dot line) corresponds to the numerical solution of (1) without (resp. with) considering the gravity term z/λ_σ^2. In (b), the solution with gravity does not predict extensions X as large as those measured.

from which we find a droplet shape close to a sinusoid.

$$\begin{pmatrix} r \\ z \\ \varphi \end{pmatrix} = \begin{pmatrix} \frac{d_v}{2}\left[1 + \varepsilon\left(1 - \cos\frac{2s}{d_v}\right)\right] \\ s \\ \frac{\pi}{2} - \varepsilon\sin\frac{2s}{d_v} \end{pmatrix}. \qquad (4)$$

The vertical extension X is equal to πd_v, which corresponds to the fibre perimeter. Both the thickness and the volume of the droplet are easily computed from (4):

$$\frac{W}{d_v} = \varepsilon = \frac{8\Omega}{\pi^2 d_v^3} \quad \text{and} \quad \frac{X}{d_v} = \pi. \qquad (5)$$

As seen in figure 3, the asymptotic laws (2) and (5) give an accurate picture of the dimensions of both large and small droplets sliding on a vertical fiber. The droplet shape has a direct influence on the sliding motion, as shown in the next section.

3.2 Short-term steady motion

The motion of a droplet on a vertical fibre involves several effects, each of them having a specific timescale. Starting from rest, the droplet first accelerates and quickly reaches (in less than 0.1 s) a limit speed V where viscous effects balance gravity, as shown indirectly in the previous subsection. The trajectory of the droplet center of mass is given by the Newton law:

$$\rho\Omega\frac{\mathrm{d}V}{\mathrm{d}t} = \rho\Omega g - F_\nu, \qquad (6)$$

where F_ν is the friction force coming out from viscous effects. This friction is due to velocity gradients within the

droplet, that Lorenceau *et al.* [15] proposed to estimate as $C_\nu V X/2Wz$. Here, z is the distance to the nearest contact line and C_ν a proportionality factor that may depend on surface tension among others. The resulting viscous force is

$$F_\nu = 2\pi d_v \int_0^{X/2} C_\nu \frac{\mu V}{z} \frac{X}{2W} \mathrm{d}z, \qquad (7)$$

where $\mu = \rho\nu$ is the dynamic viscosity of the droplet. This integral diverges due to the singularity at contact point ($z = 0$). In order to solve this paradox, De Gennes [7] proposed to integrate from $z = a \sim 10^{-9}$ m – the characteristic length of the molecular film covering the fibre – instead of $z = 0$. This yields

$$F_\nu = \pi C_\nu \alpha \mu d_v \frac{X}{W} V, \qquad (8)$$

where

$$\alpha = \ln(X/2a) \simeq 15. \qquad (9)$$

Balancing this force with the droplet weight $\rho g\Omega$ gives

$$\frac{\nu V}{g d_v^2} = \frac{1}{\pi C_\nu \alpha} \frac{W}{X} \frac{\Omega}{d_v^3}. \qquad (10)$$

A similar scaling is found in [16] and [9]. As previously seen (Fig. 3), the dependence of W/X on Ω/d_v^3 is complex in the general case, but droplets sufficiently large compared to the fibre tend to be spherical so $W/X \to 0.5$. Equation (10) is in excellent agreement with experimental results (Fig. 4), whatever the fibre diameter d_v, provided that C_ν satisfies

$$C_\nu = c_\nu\sqrt{\frac{\lambda_\sigma}{d_v}} \Rightarrow \frac{\nu V}{g d_v^2} = \pi c_\nu \alpha\sqrt{\frac{d_v}{\lambda_\sigma}} \frac{W}{X} \frac{\Omega}{d_v^3}. \qquad (11)$$
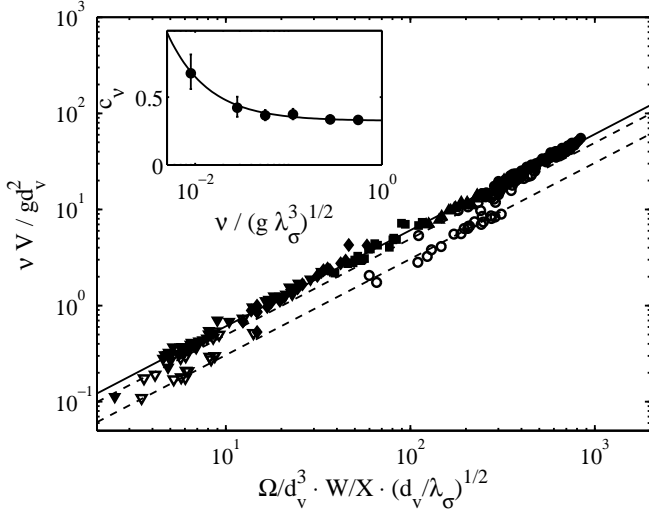
Fig. 4. Short-term balance: normalized velocity $\nu V/gd_v^2$ as a function of the normalized volume Ω/d_v^3. Black (resp. white) symbols correspond to viscosity $\nu \geq 10$ cS (resp. $\nu < 10$ cS). (○,●) $d_v = 80$ μm, (▲) $d_v = 100$ μm, (■) $d_v = 140$ μm, (◆) $d_v = 200$ μm, (▼,▽) $d_v = 250$ μm. The solid line represents Eq. (11) where c_ν takes its high-viscosity value (0.33). The dashed line is Eq. (11) in the low-viscosity regime, i.e. $c_\nu > 0.33$. (Inset) Coefficient c_ν as a function of the normalised viscosity $\nu/\sqrt{g\lambda_\sigma^3}$. The solid line corresponds to Eq. (12).

The factor $\sqrt{d_v/\lambda_\sigma}$ clearly indicates that gravity is not perfectly balanced by viscous effects, and that surface tension also plays a role in the droplet limit velocity. The coefficient c_ν is of the order of unity; it slightly depends on the viscosity when this one is lower than 10 cS. The following empirical law is proposed to fit the measurements (inset of Fig. 4),

$$c_\nu = 0.33\left(1 + 0.01\frac{\sqrt{g\lambda_\sigma^3}}{\nu}\right). \qquad (12)$$

The viscosity ν is here made dimensionless by the factor $\sqrt{g\lambda_\sigma^3}$, which only involves g, σ and ρ.

We can now estimate the acceleration time of the droplet from Eq.(6):

$$t_a \sim \frac{V}{g} = \frac{1}{\pi c_\nu \alpha}\sqrt{\frac{d_v}{\lambda_\sigma}}\frac{W}{X}\frac{\Omega}{d_v\nu}, \qquad (13)$$

and check that, for a maximal velocity of 1 m/s, the steady regime is reached after 0.1 s. The balance (10) between gravity and viscous forces is therefore quickly effective, it determines the droplet velocity along the fiber.

3.3 Long-term mass loss

The coating of a solid by a liquid has been deeply investigated since the pioneering work of Landau and Levich [12]. The so-called LLD theory rationalises the coating of

a plate slowly pulled out of a liquid bath. It was generalized later to other geometries, including a fiber pulled out from a bath ([19] and references therein). In that case, the thickness δ of the coating film is given by

$$\frac{\delta}{d_v} = c_w Ca^{2/3} \quad \text{with} \quad Ca = \frac{\mu V}{\sigma}, \qquad (14)$$

where Ca is the capillary number and the wetting constant $c_w = 0.67$ according to the authors. Many corrections (gravity, inertia, geometry, wetting, etc.) can be implemented by simply changing this factor c_w [19]. For example, $c_w = 1.07$ when the fibre crosses the interface between two immiscible liquids [1, 2].

Sliding droplets are observed to coat fibres in the same way as if these latter were pulled out of a bath. Consequently, the droplets lose some mass through coating and progressively slow down as they move on the fibre. Equation (14) may be applied to predict the mass loss and be coupled to (11) in order to get the long-term trajectory of the droplet. Denoting by Z the vertical position of the droplet mass centre (so $\dot{Z} = V$), the volume variation $\dot{\Omega}$ is

$$\dot{\Omega} = -\pi d_v \delta \dot{Z} = -\pi c_w d_v^2\left(\frac{\mu}{\sigma}\right)^{2/3}\dot{Z}^{5/3}. \qquad (15)$$

We proceed by differentiating (11) with respect to time, supposing that W/X is constant:

$$\dot{\Omega} = \pi c_\nu \alpha \frac{X}{W}\sqrt{\frac{\lambda_\sigma}{d_v}}\frac{\nu d_v \ddot{Z}}{g}. \qquad (16)$$

Both equations yield

$$\ddot{Z} = -w\dot{Z}^{5/3} \text{ with } w = -\frac{c_w}{c_\nu \alpha}\frac{W}{X}\sqrt{\frac{d_v}{\lambda_\sigma}}\left(\frac{\mu}{\sigma}\right)^{2/3}\frac{gd_v}{\nu}, \quad (17)$$

where the parameter w only depends on physical constants. This equation is integrated twice;

$$Z = \frac{\dot{Z}_i^{1/3} - \left(\dot{Z}_i^{-2/3} + \frac{2}{3}wt\right)^{-1/2}}{w/3}, \qquad (18)$$

where $\dot{Z}_i$ is the initial velocity of the droplet. The long-term trajectory (vertical position on the fiber as a function of time) is measured for droplets with various parameters (size and viscosity). The experimental results are compared to the predictions of Eq. (18) in Fig. 5. The initial velocity $\dot{Z}_i$ is fitted on the experiments, and w is computed by successively taking $c_w = 0.67$ and $c_w = 1.5$. This second value gives an accurate description of the long-term trajectory, whatever the droplet viscosity or size. Finally, we check a posteriori that the ratio W/X is approximately constant during the measurement period. Typically, W/X variations become significant when Ω is varied by a factor 10, which happens after about $5.5/(w\dot{Z}_i^{2/3})$, i.e. after 89 s for the (▼)-curve in Fig. 5.
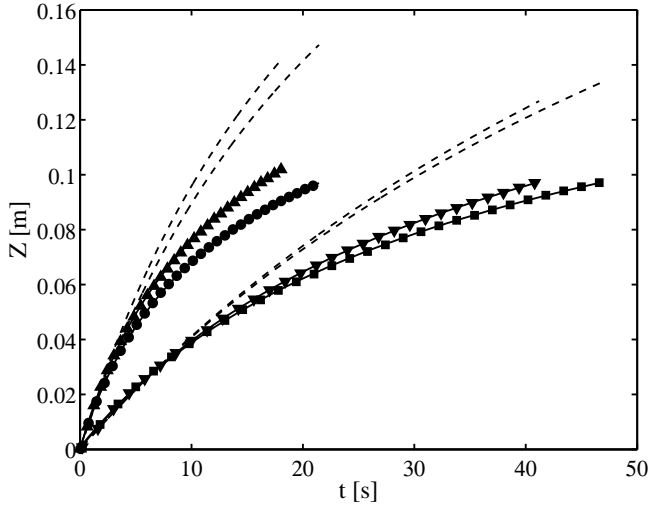
Fig. 5. Long-term trajectories $Z(t)$ of droplets with various viscosities and initial sizes on a fibre of diameter $d_v = 250\ \mu$m: (●) $\nu = 10$ cS, (▲) $\nu = 20$ cS, (■) $\nu = 50$ cS, and (▼) $\nu = 100$ cS. The solid line (resp. dashed line) corresponds to Eq. (18) in which $c_w = 1.5$ (resp. $c_w = 0.67$). The initial velocity $\dot{Z}_i$ in Eq. (18) is fitted on the experimental data.

3.4 Shape transition

The droplet shape on a fibre is not always axisymmetric and unique; several equilibrium configurations may coexist, some being more stable than others [17]. We have seen that some 100 cS droplets sliding on a vertical fibre can remain in a metastable asymmetrical shape. At any moment, these droplets quickly switch to the well-known axisymmetrical configuration. By the way, the friction is considerably increased and the droplets immediately slow down (Fig. 6a). The inverse transition has never been observed and is likely impossible. The transition point seems to be arbitrary, the exact nature of the transition is still unknown.

The velocity V_f of the final symmetrical shape has been measured as a function of the initial velocity V_i before the transition, for 100 cS droplets on various fibres (Fig. 6b). Data suggest

$$V_f \simeq 0.30 V_i, \qquad (19)$$

so the friction coefficient c_ν is about 3.3 times less in the asymmetrical configuration.

We have observed a similar transition on inclined fibres, though both configurations are asymmetric in that case (Fig. 7). The centre of mass of the droplet slightly moves toward the fiber, which leads to increased velocity gradients and consequently an increase in the friction force. However, the resulting velocity is only decreased by a factor 2 during the transition.
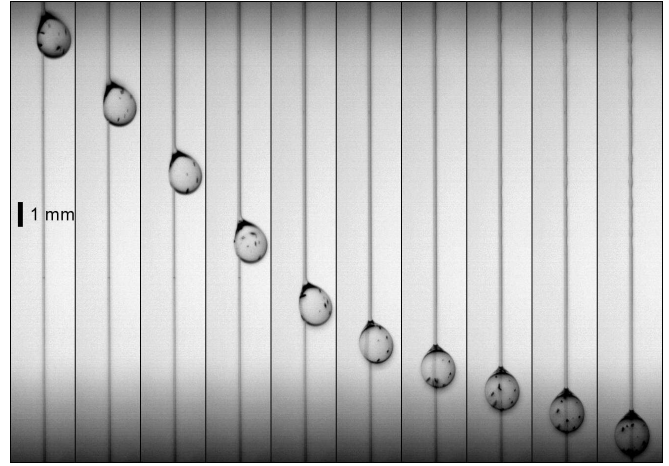
(a)
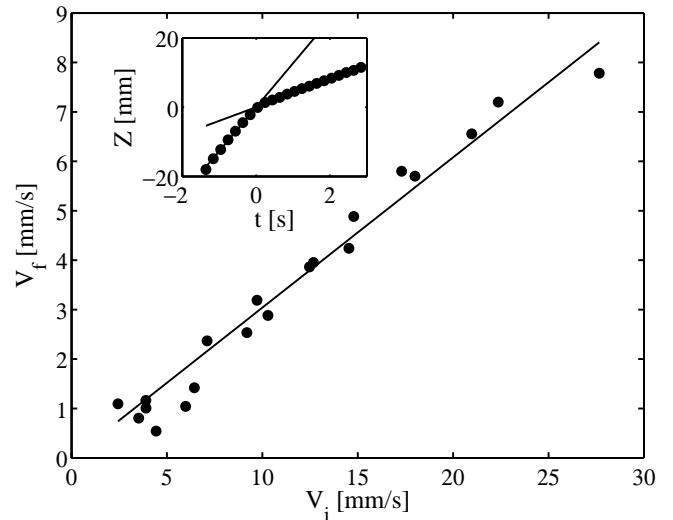
(b)

Fig. 6. (a) A 100 cS droplet slides along a vertical fibre of diameter $d_v = 160\ \mu$m. Snapshots are taken every 160 ms. The initially asymmetrical shape suddenly becomes symmetric, which decreases the droplet velocity from 18 mm/s to 5.7 mm/s. (b) Velocity of the symmetrical shape V_f as a function of the velocity of the corresponding asymmetrical shape V_i. The solid line corresponds to Eq. (19). (Inset) Typical trajectory $Z(t)$ of a droplet experiencing a shape transition in $t = 0$. The solid lines represent constant velocity trajectories.

4 Intersection between two fibres

We proceed by discussing the behaviour of droplets as they encounter an intersection between two fibres. The junction is simply made by placing a horizontal fibre next to the vertical one so they just touch each other; contact is ensured by the tension of both fibres.

Droplets are released on the vertical fibre, upstream from the intersection. As already noted in [9], two scenarios are observed: small droplets remain pinned on the node (Fig. 8a) while larger droplets cross the intersection and keep sliding downwards (Fig. 8b). The trapping of small
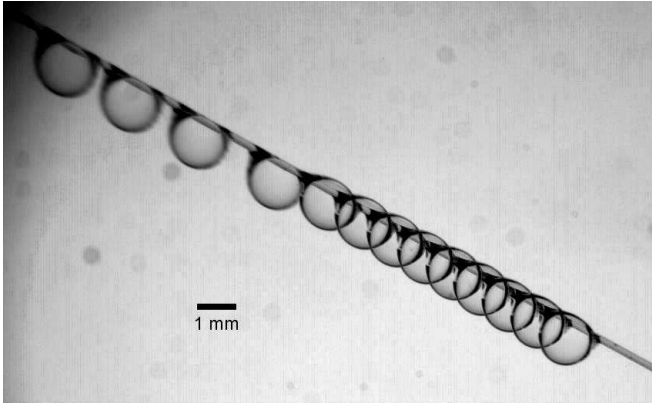
Fig. 7. A 100 cS droplet slides along an inclined fibre of diameter $d_v = 140\,\mu$m. Snapshots are taken every 320 ms and superposed together. The shape transition increases the friction, so decreasing the velocity from 6 mm/s to 3 mm/s.

droplets is mainly due to the capillary forces developed by the horizontal fibre. On the other hand, large droplets are likely too heavy to hang on the horizontal fibre. Lorenceau *et al.* [15] have already investigated a problem that involve nearly the same mechanism, i.e. falling droplets that impact a horizontal fibre. We note however that droplets in free fall have a much larger velocity, so in addition the droplet inertia has to be considered.

The balance between gravity and surface tension is the Bond number related to the fibre, defined as

$$Bo = \frac{\rho \Omega g}{2\pi \sigma d_h}, \qquad (20)$$

where d_h is the diameter of the horizontal fibre. A sharp transition is observed between blocking and crossing regimes (Fig. 9a); there is a critical Bond number $Bo^*\sim 1$ above which droplets cross the node and below which they are blocked. The intersection behaves as a fluidic diode. This Bo^* depends on the droplet viscosity ν, at least when this latter is small.

When crossing, a tiny amount of liquid is still trapped by the horizontal fibre, so the droplet mass (and corresponding Bond number Bo_f) after crossing is slightly lower than before (Bo_i). Although this volume cannot be accurately measured, it should scale as the "volume" of the intersection, namely $d_h d_v (d_h + d_v)$.

Large high viscosity droplets may experience significant delays (sometimes as long as several seconds) when they cross the intersection (Fig. 10). This delay time t_h is shown to diverge as $Bo \to Bo^*$, as often in physics when a potential barrier is just crossed (Fig. 9b). According to the experimental data, t_h is proportional to the kinematic viscosity ν of the droplet, so the data collapse on a single curve when the dimensional group t_h/ν (measured in $s^2 m^{-2}$) is represented instead of t_h. Note that the divergence is not observed for low viscosity droplets whose crossing time remains small.

As already seen in Fig. 9, the threshold Bond number Bo^* increases with the droplet viscosity, and saturates to
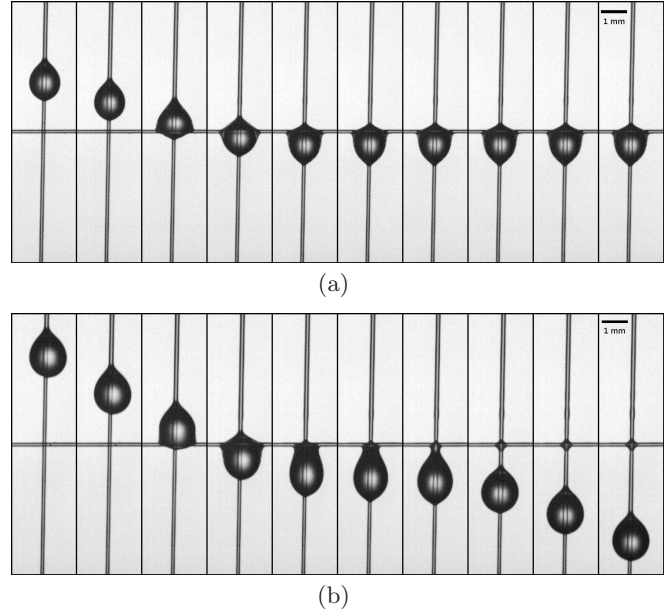

(a)

(b)

Fig. 8. A 5 cS oil droplet interacts with a junction between two nylon fibres (diameter 140 μm). Snapshots are taken every 10 ms. The intersection behaves as a fluidic diode: (a) A small droplet is pinned on a junction that (b) a large droplet is able to cross. In that latter case, a tiny amount of liquid is left at the intersection.

a limit value in the high viscosity regime where delays are observed. The critical viscosity above which Bo^* is constant depends on the fibre diameter (Fig. 11a). In general, Bo^* decreases with increasing fibre diameter (Fig. 11b) in a non-obvious way.

4.1 Modelling

In order to model the behaviour of a droplet interacting with a junction between two fibres, we have first to measure and analyse the droplet trajectory. Observations are again qualitatively different depending on the viscosity regime. As already mentioned, high viscosity droplets cross the junction with a delay time that increases as they approach the threshold Bo^* (Fig. 12a). Small droplets are smoothly blocked, and the trajectory is always monotonic. Low viscosity droplets do not experience any significant delay when crossing is allowed. Moreover, small blocked droplets largely oscillate before coming to rest on the node (Fig. 12b).

These experimental results strongly suggest to model the droplet as a damped harmonic oscillator whose restoring force is truncated to the neighbourhood of the node. Assuming that the position Z of the droplet mass centre is counted from the intersection (thus corresponding to $Z = 0$), we introduce a characteristic function $\chi_{[-Z_1, Z_2]}(Z)$ equal to 1 when $-Z_1 < Z < Z_2$ and 0 otherwise. The droplet starts touching the node when $Z = -Z_1 < 0$ and detaches in $Z = Z_2 > 0$. The governing equation for this truncated
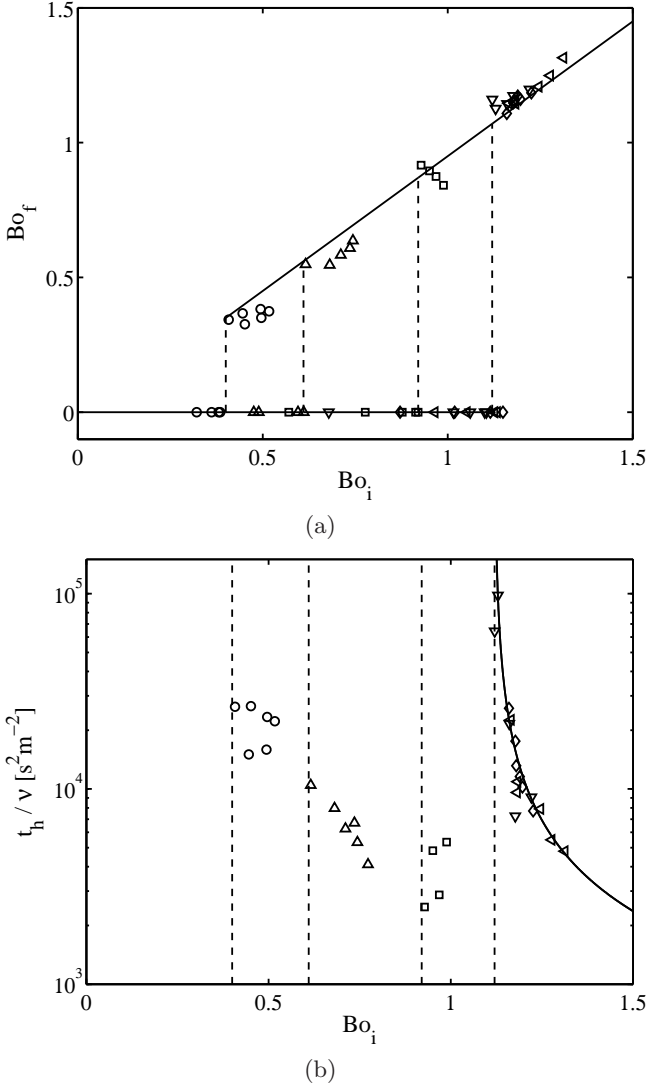
(a)

(b)

Fig. 9. (a) Relationship between the volume of liquid allowed to cross the node and the initial droplet volume, expressed in terms of Bond numbers $Bo_f(Bo_i)$. The solid lines correspond to equations $Bo_f = 0$ when $Bo_i < Bo^*$ (blocking) and $Bo_f = Bo_i - 0.05$ when $Bo_i > Bo^*$ (crossing). (b) Time t_h[s] needed by the droplet to cross the intersection, as a function of Bo_i. The solid line is the empirical law $t_h/\nu = 900/(Bo_i - Bo^*)$, where the dimensional prefactor is 900 s^2 m^{-2}. (a-b) Experimental data for $d_h = 250\,\mu$m and $d_v = 80\,\mu$m: (○) $\nu = 1.5$ cS, (△) $\nu = 5$ cS, (□) $\nu = 10$ cS, (▽) $\nu = 20$ cS, (◇) $\nu = 50$ cS and (◁) $\nu = 100$ cS. Error bars typically correspond to the symbol size. The dashed lines correspond to the Bo^* values.

oscillator is

$$\rho\Omega\ddot{Z} + C_\mu\mu\Omega^{1/3}\dot{Z} + kZ\chi_{[-Z_1,Z_2]}(Z) = \rho\Omega g, \qquad (21)$$

where C_μ is the friction coefficient and k is the stiffness of the spring mechanism related to the horizontal fibre, so

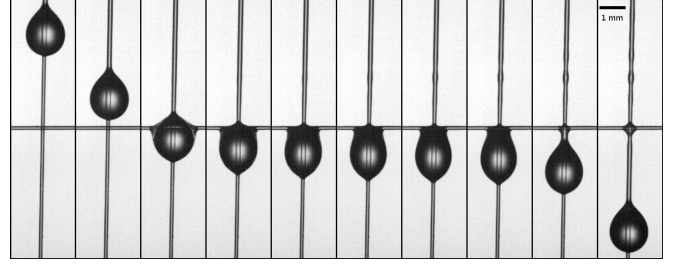$$k = c_\sigma \frac{d_h}{\Omega^{1/3}}\sigma, \qquad (22)$$

Fig. 10. A delay of about 0.5 s is observed when a 50 cS droplet with $Bo \to Bo^*$ crosses the intersection between two fibres of diameter 140 μm. Snapshots are taken every 120 ms.
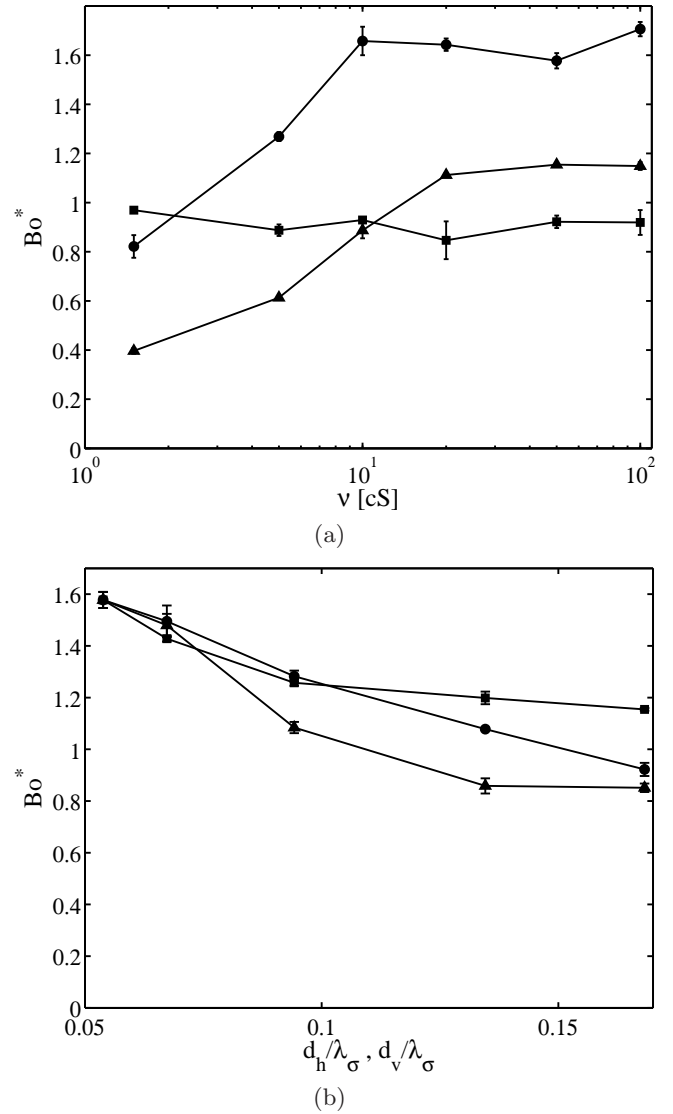

(a)

(b)

Fig. 11. (a) Variation of Bo^* with the droplet viscosity ν for (●) $d_h = d_v = 80\,\mu$m, (■) $d_h = 80\,\mu$m and $d_v = 250\,\mu$m, and (▲) $d_h = 250\,\mu$m and $d_v = 80\,\mu$m. (b) Variation of Bo^* with the fibre diameters, for $\nu = 50$ cS. (●) $d_h = 80\,\mu$m and d_v is varied, (■) $d_v = 80\,\mu$m and d_h is varied, and (▲) $d_h = d_v$ are both varied.

(a)

(b)

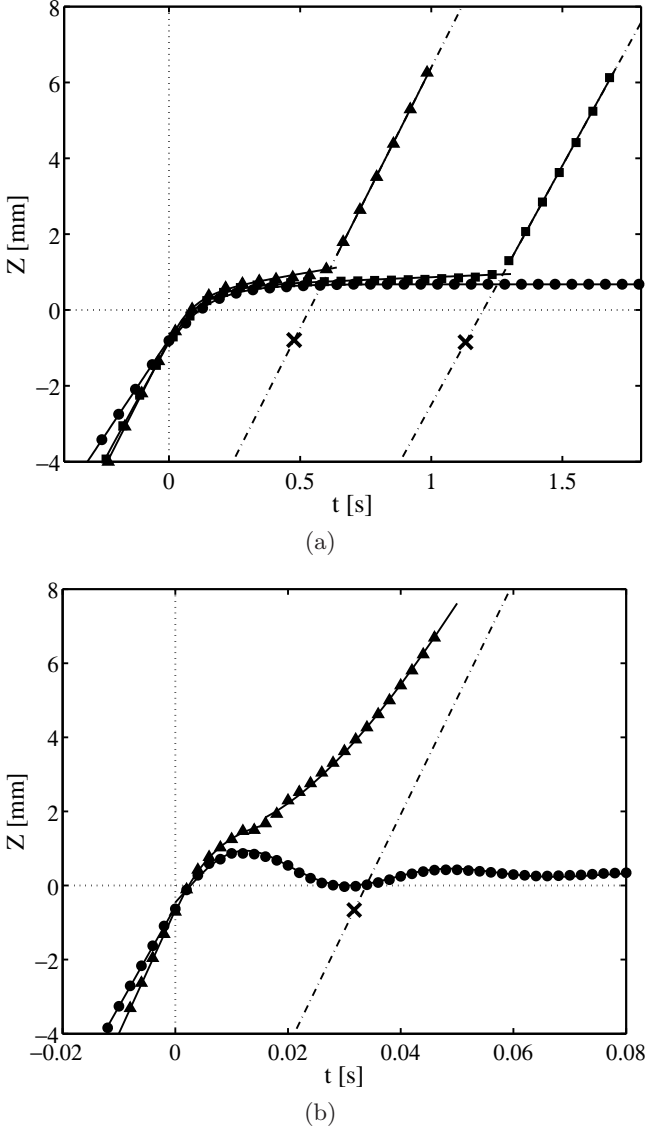**Fig. 12.** (a) Droplet trajectory in the high-viscosity regime, namely for $d_h = d_v = 80\ \mu$m and $\nu = 100$ cS, so $Bo^* \simeq 1.67$. (●) Blocking for $Bo_i = 1.54$, (▲) crossing for $Bo_i = 1.87$, and (■) crossing with delay for $Bo_i = 1.68$. (b) Droplet trajectory in the low-viscosity regime, namely for $d_h = 250\ \mu$m, $d_v = 80\ \mu$m and $\nu = 1.5$ cS, so $Bo^* \simeq 0.41$. (●) Blocking for $Bo_i = 0.38$, and (▲) crossing for $Bo_i = 0.52$. In both (a) and (b), the solid line corresponds to the fit of Eq. (21), while the dash-dot line represents the linear trajectory that the droplet would have taken if it had not been delayed by the horizontal fibre. The cross indicates the delay time t_h.

where c_σ is the stiffness coefficient. Both C_μ and c_σ have to be estimated from experimental measurements.

Equation (21) is put in a dimensionless form by using

$$y = Z/Z_1 \tag{23}$$

and $\tau = \sqrt{k/M}t$;

$$\ddot{y} + 2\beta\dot{y} + y\chi_{[-1,\kappa]}(y) = \Theta, \tag{24}$$

where

$$\kappa = Z_2/Z_1,\ \beta = \frac{C_\mu}{\sqrt{c_\sigma}}\frac{\mu}{\sqrt{\rho\sigma d_h}}\ \text{and}\ \Theta = \frac{\rho\Omega g}{kZ_1} = \frac{2\pi\Omega^{1/3}}{c_\sigma Z_1}Bo. \tag{25}$$

We note that the damping factor β is equivalent to an Ohnesorge number based on d_h, and the forcing parameter Θ is proportional to the Bond number.

This equation may be solved starting from the initial conditions $y(0) = -1$ and $\dot{y}(0) = \Theta/2\beta$, i.e. when the droplet, evolving at the limit speed $\Theta/2\beta$ as described in sec. 3, touches the horizontal fibre. As in the classical damped oscillator, two regimes are observed in Eq. (24) according to the value of β. For $\beta > 1$, the system is overdamped and corresponds to the high-viscosity regime, while it is underdamped otherwise.

In the overdamped regime $\beta > 1$, the solution is

$$y(\tau) = \Theta - e^{-\beta\tau}\left[(1+\Theta)\cosh(\omega\tau) + \frac{2\beta^2(1+\Theta) - \Theta}{2\beta\omega}\sinh(\omega\tau)\right], \tag{26}$$

where

$$\omega = \sqrt{|\beta^2 - 1|}. \tag{27}$$

The solution always tends monotonically towards $y = \Theta$. Nevertheless, the solution is not valid anymore when $y > \kappa$ due to the truncation; $\Theta^* = \kappa$ is therefore the threshold that separates blocking ($\Theta < \kappa$) and crossing ($\Theta > \kappa$) behaviours. The crossing time obviously diverges when $\Theta \to \kappa^+$, as in experiments.

In the underdamped regime $\beta < 1$, the solution is

$$y(\tau) = \Theta - e^{-\beta\tau}\left[(1+\Theta)\cos(\omega\tau) + \frac{2\beta^2(1+\Theta) - \Theta}{2\beta\omega}\sin(\omega\tau)\right]. \tag{28}$$

The solution also tends towards $y = \Theta$, but with damped oscillations. The critical point $y = \kappa$ is necessarily reached at the first oscillation, so the crossing delay cannot be larger than the oscillator period. The blocking/crossing threshold Θ^* is obtained when the first maximum of Eq. (28) coincides with $y = \kappa$, which yields

$$y(\tau^*, \Theta^*) = \kappa \quad \text{with} \quad \tan(\omega\tau^*) = \frac{-\Theta^*\omega}{\beta(\Theta^* + 2)}, \tag{29}$$

where τ^* is the time of first maximum when $\Theta = \Theta^*$. This system of implicit equations with unknowns (τ^*, Θ^*) cannot be solved analytically. Nevertheless, it can be shown that $(\tau^*, \Theta^*) \to (\pi, 0)$ when $\beta \to 0$.

When crossing occurs and y passes the κ-point in τ_κ, the droplet starts accelerating again until it reaches its terminal velocity:

$$y(\tau) = \kappa + \frac{\Theta}{2\beta}(\tau - \tau_\kappa) - \frac{\Theta - 2\beta\dot{y}(\tau_\kappa)}{4\beta^2}\left[1 - e^{-2\beta(\tau - \tau_\kappa)}\right], \tag{30}$$

where $\dot{y}(\tau_\kappa)$ is the velocity at the exit point $y = \kappa$.

Equations perfectly fit experimental trajectories (Fig. 12). As seen in Fig. 13, the fitting parameters C_μ and c_σ ap-

	$d_h = 80~\mu$m	$d_h = 250~\mu$m
c_μ	$13 \pm 20\%$	$27 \pm 12\%$
c_σ	$16 \pm 18\%$	$9.9 \pm 22\%$

proximately satisfy

$$
\begin{cases}
C_\mu = c_\mu\left(\dfrac{d_h}{\lambda_\sigma}, \dfrac{d_v}{\lambda_\sigma}\right)\dfrac{\lambda_\sigma^3}{\Omega}, \\[2mm]
c_\sigma = c_\sigma\left(\dfrac{d_h}{\lambda_\sigma}, \dfrac{d_v}{\lambda_\sigma}\right).
\end{cases}
\tag{31}
$$

The coefficients c_μ and c_σ are given in Table 4.1 for various d_h and for $d_v = 80~\mu$m, Dimensionless parameters Θ and β are computed for each experiment, starting from these values of c_μ and c_σ. The agreement with the theoretical equation (29) is rather good (Fig. 14), considering the significant error made by converting the measured physical parameters into dimensionless quantities β and Θ [1].

Finally, we note that the parameter c_σ may be related to the critical Bond number Bo^*. Indeed, in the over-damped regime, $\Theta^* = \kappa$, so

$$
Z_2 = 4\pi \frac{\Omega^{*1/3}}{c_\sigma} Bo^*_{\nu\to\infty}.
\tag{32}
$$

Measurements of $Bo^*(d_h, d_v)$ (directly from the experiments) and $c_\sigma(d_h, d_v)$ (from the trajectory fitting) suggest that $Z_2 = 0.68\Omega^{1/3}$, whatever d_h and d_v. Therefore,

$$
c_\sigma \simeq 9.24 Bo^*_{\nu\to\infty}.
\tag{33}
$$

5 Conclusion

In this paper, we have discussed the behaviour of silicon oil droplets that slide along a vertical fibre and intercept a horizontal fibre. The shape and the trajectory of the droplets were measured experimentally. The size of both the droplet and the fiber was varied, as well as the droplet viscosity.

On a vertical fibre, the axisymmetric shape of the droplet is shown to be close to an unduloid, namely the solution of Laplace equation when gravity is not taken into account. Indeed, gravity is balanced by viscous stresses when the droplet slides along the fibre; this balance sets the droplet velocity. Asymmetric shapes were observed, with a smaller friction coefficient and a consequently greater velocity. However, these configurations are unstable and the droplets quickly switch to the axisymmetric configuration. As they slide down, the droplets leave a coating film in their wake, on the fibre. Consequently, they lose some mass so they slowly decelerate.

Large droplets are observed to cross the intersection between two fibres, while smaller ones are blocked at the junction. The threshold size is prescribed by a Bond number, namely a balance between the droplet weight and

---

[1] Relative errors from each variables and fitting parameters are summed when multiplying the variable to get dimensionless parameters.
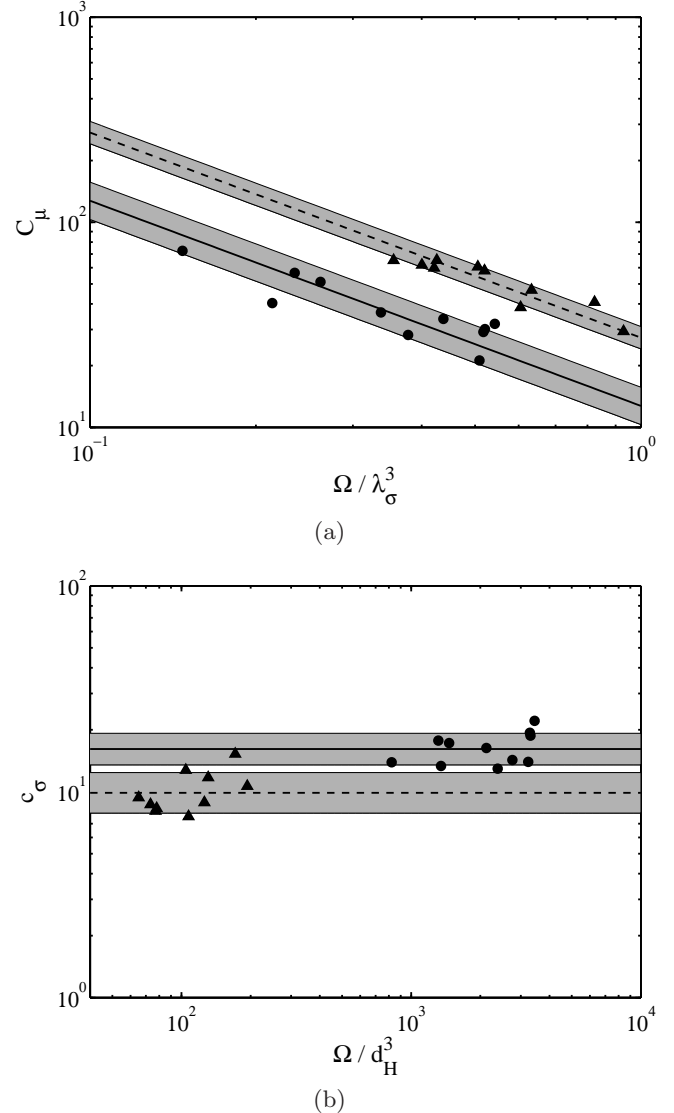

Fig. 13. Coefficients C_μ and c_σ of the dimensional model (21). Symbol data are obtained by fitting this model to the experimental trajectories. The lines correspond to Eq. (31), the shaded areas represent standard deviations. The ($\bullet$) and solid line (resp. ($\blacktriangle$) and dashed line) correspond to $d_h = 80~\mu$m (resp. $d_h = 250~\mu$m), while $d_v = 80~\mu$m in both cases.

the capillary force mainly exerted by the horizontal fibre. This number is shown to increase with increasing viscosity; a saturation is observed at high viscosity. The blocking vs. crossing transition has been rationalised, starting from the Newton law for the centre of mass of the droplet. The resulting differential equation is equivalent to a damped harmonic oscillator, for which the restoring force is truncated to the neighbourhood of the junction. The parameters of the model are deduced by fitting the solutions of the differential equation on the measured trajectories. The model predictions are in very good agreement with the experimental observations.
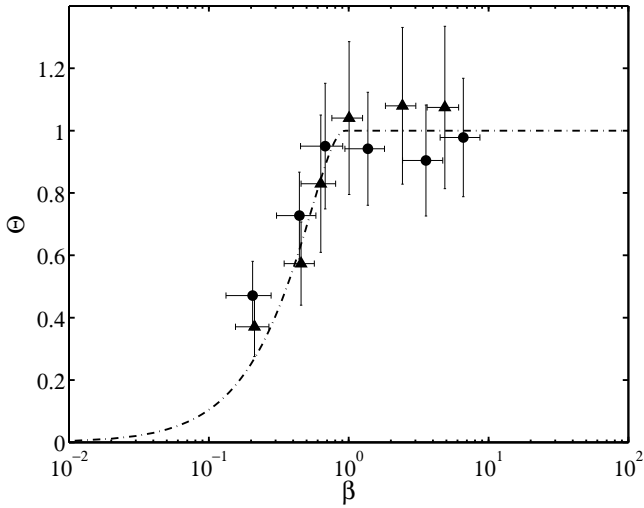
Fig. 14. Dimensionless threshold curve $\Theta(\beta)$ given by Eq. (29). Symbols represent the experimental data for $d_v = 80~\mu$m and (•) $d_h = 80~\mu$m or (▲) $d_h = 250~\mu$m. The conversion from dimensional measurements to dimensionless variables is made through Eq. (25).

In a recent paper [9], it has been shown that droplets may be divided into N micro-droplets by using a fibre network made of one vertical fibre and N horizontal fibres. The initial droplet is sufficiently large to cross every junction. The coating film left in its wake destabilises into small pearls that are progressively collected at the N nodes since they are usually too small to cross them. The droplet division is the key step towards multiplexing and more complex microfluidic operations [14, 24, 23]. Consequently, a microfluidic technology based on fibres may be a promising way to handle droplets for biochemical uses. It is hoped that our study will inform ongoing investigations and developments of droplets on fibre networks.

References

1. P. Aussillous and D. Quéré. Quick deposition of a fluid on the wall of a tube. *Phys. Fluids*, 12(10):2367, 2000.
2. J. Bico and D. Quéré. Self-propelling slugs. *J. Fluid Mech.*, 467:101, 2002.
3. B.J. Carroll. The accurate measurement of contact angle, phase contact areas, drop volume, and laplace excess pressure in drop-on-fiber systems. *J. Colloid Interface Sci.*, 57(3):488, 1976.
4. P. Contal, J. Simao, D. Thomas, T. Frising, S. Callé, J.C. Appert-Collin, and D. Bémer. Clogging of fibre filters by submicron droplets. phenomena and influence of operating conditions. *Aerosol Science*, 35:263, 2004.
5. R.V. Craster and O.K. Matar. On viscous beads flowing down a vertical fibre. *J. Fluid Mech.*, 553:85, 2006.
6. S. Dawar, H. Li, J. Dobson, and G.G. Chase. Drag correlation of drop motion on fibers. *Drying technology*, 24:1283, 2006.
7. P.G. de Gennes. Wetting: statics and dynamics. *Rev. Mod. Phys.*, 57(3):827, 1985.
8. C. Duprat, C. Ruyer-Quil, S. Kalliadasis, and F. Giorgiutti-Dauphiné. Absolute and convective instabilities of a viscous film flowing down a vertical fiber. *Phys. Rev. Lett.*, 98:244502, 2007.
9. T. Gilet, D. Terwagne, and N. Vandewalle. Digital microfluidics on a wire. *Appl. Phys. Lett.*, 95:014106, 2009.
10. I.L. Kliakhandler, S.H. Davis, and S.G. Bankoff. Viscous beads on vertical fibre. *J. Fluid Mech.*, 429:381, 2001.
11. A. Kumar and S. Hartland. Shape of a drop on a vertical fiber. *J. Colloid Interface Sci.*, 124(1):67, 1988.
12. L.D. Landau and B. Levich. Dragging of a liquid by a moving plate. *Acta Physicochim. USSR*, 17:42, 1942.
13. N. LeGrand, A. Daerr, and L. Limat. Shape and motion of drops sliding down an inclined plane. *J. Fluid Mech.*, 541:293, 2005.
14. D.R. Link, S.L. Anna, D.A. Weitz, and H.A. Stone. Geometrically mediated breakup of drops in microfluidic devices. *Phys. Rev. Lett.*, 92:054503, 2004.
15. E. Lorenceau, C. Clanet, and D. Quéré. Capturing drops with a thin fiber. *J. Colloid Interface Sci.*, 279:192, 2004.
16. E. Lorenceau and D. Quéré. Drops on a conical wire. *J. Fluid Mech.*, 510:29, 2004.
17. G. McHale and M.I. Newton. Global geometry and the equilibrium shapes of liquid drops on fibers. *Colloids and Surfaces A: Physicochem. Eng. Aspects*, 206:79, 2002.
18. J. Plateau. *Statique exprimentale et thorique des liquides soumis aux seules forces molculaires.* Paris: Gauthier-Villars, 1873.
19. D. Quéré. Fluid coating on a fiber. *Annu. Rev. Fluid Mech.*, 31:347, 1999.
20. Lord Rayleigh. On the capillary phenomena of jets. *Proc. Roy. Soc. London*, 29:71, 1879.
21. S. N. Reznik, W. Salalha, A.L. Yarin, and E. Zussman. Microscale fibre alignment by a three-dimensional sessile drop on a wettable pad. *J. Fluid Mech.*, 574:179, 2007.
22. S.N. Reznik and A.L. Yarin. Spreading of a viscous drop due to gravity and capillarity on a horizontal or an inclined dry wall. *Phys. Fluids*, 14(1):118, 2002.
23. T. Squires and S.R. Quake. Microfluidics: Fluid physics at the nanoliter scale. *Rev. Mod. Phys.*, 77:977, 2005.
24. H.A. Stone, A.D. Stroock, and A. Ajdari. Engineering flows in small devices : Microfluidics towards a lab-on-a-chip. *Annu. Rev. Fluid Mech.*, 36:381, 2004.
25. A. L. Yarin, W. Liu, and D. H. Reneker. Motion of droplets along thin fibers with temperature gradient. *J. Appl. Phys.*, 91(7):4751, 2002.

26. A.L. Yarin, G.G. Chase, W. Liu, S.V.Doiphode, and
    D.H. Reneker. Liquid drop growth on a fiber. *AIChE
    Journal*, 52(1):217, 2006.
27. A.L. Yarin, A. Oron, and Ph. Rosenau. Capillary in-
    stability of thin liquid film on a cylinder. *Phys. Fluids
    A*, 5(1):91, 1993.